The Effect of Lesion Size and Activity Concentration on Image Quality in PET/CT Imaging: A Phantom Study

A. Karayel[a,*], R.T. Güray[b], C. Yalçın[b], N. Yeyin[c], S. Coşkun[c], S. İşgören[a], G. Dağlıöz[a], H. Demir[a], H.O. Tekin[d] and M. Demir[c]

[a]*Kocaeli University, Medical Faculty, Department of Nuclear Medicine, Izmit, 41001 Kocaeli, Turkey*
[b]*Kocaeli University, Faculty of Arts and Science, Department of Physics, Izmit, 41000 Kocaeli, Turkey*
[c]*Istanbul University-Cerrahpasa, Medical Faculty, Department of Nuclear Medicine, Fatih, 34098 İstanbul, Turkey*
[d]*Istinye University, Faculty of Engineering and Natural Sciences, Sarıyer, 34396 İstanbul, Turkey*

Received: 02.09.2025 & Accepted: 03.11.2025

Doi: 10.12693/APhysPolA.148.220 *e-mail: karayel.ahmet@kocaeli.edu.tr

In this study, the National Electrical Manufacturers Association (NEMA) image quality tests were conducted using the General Electric Discovery 690 model — a hybrid system of positron emission tomography/computed tomography. Quantitative evaluation of image quality within this model primarily involves the use of parameters such as contrast (C), contrast-to-noise ratio (CNR), and contrast recovery coefficient (CRC). These metrics are considered essential performance indicators, particularly in standardized assessment protocols such as those proposed by NEMA. The objective of this study was to evaluate image quality in a NEMA positron emission tomography phantom using ^{18}F-FDG at different signal-to-background (S/Bg) ratios and varying activity concentrations, and to determine the minimum detectable lesion size. Positron emission tomography images were acquired using a NEMA 2012/IEC 2008 phantom with ^{18}F-FDG at S/Bg ratios of 4:1, 6:1, and 8:1, across decreasing activity concentrations ranging from 9.98 to 1.93 MBq/kg. At an S/Bg ratio of 4:1, activity concentrations below 3.90 MBq/kg (as well as at 6:1 below 2.76 MBq/kg) resulted in CNR values less than 5, falling below the detectability threshold. Regarding the CRC [%] values, for the 4:1 ratio, lesions with diameters of 13 and 10 mm fell outside the acceptable limits at concentrations below 2.89 MBq/kg. Similarly, for the 6:1 ratio, lesions with a diameter of 10 mm exceeded these limits at concentrations below 5.29 MBq/kg. Multiple acquisitions were performed at different ratios and activity levels, and the lesion detectability for each condition was determined based on the Rose criterion (CNR ≥ 5).

topics: positron emission tomography (PET) image quality, PET image quality (IQ) phantom, C and CNR and CRC

1. Introduction

Positron emission tomography is an advanced molecular nuclear medicine imaging modality that enables the evaluation of metabolic processes. Positron emission tomography/computed tomography (PET/CT) imaging, most commonly performed using F-18 fluorodeoxyglucose (^{18}F-FDG), is widely applied in a variety of clinical fields, particularly oncology, as well as neurology and cardiology. Although various positron-emitting radiopharmaceuticals are used in PET/CT imaging, ^{18}F-FDG remains one of the most frequently utilized. The radionuclide ^{18}F has a physical half-life of 109.8 min and a maximum positron energy of 0.635 MeV; it is cyclotron-produced and commercially available [1].

Image quality (IQ) evaluation is critical for improving diagnostic accuracy, optimizing system performance, and determining the optimal activity of administered radiopharmaceuticals for patients. In PET/CT imaging, inadequate image quality may lead to false-negative or false-positive results, particularly in cases requiring precise assessments, such as small lesion detection and staging, which may result in erroneous clinical decisions and treatment planning [2].

Recent technological advancements in PET/CT imaging have significantly improved scanner performance, particularly in terms of axial field of view (FOV) and system sensitivity. Long-axial FOV systems offer up to (10–40)× higher sensitivity, enabling improved count statistics even at reduced activity levels [3]. In addition, artificial

intelligence (AI)-assisted image reconstruction techniques have begun to transform PET imaging workflows.

The key to the success of this technique is the combination of various physical parameters, including image quality, contrast, spatial resolution, noise level, sensitivity, and accuracy, which are determined using phantoms [4, 5].

Among the principal metrics used to quantitatively assess PET/CT image quality are contrast (C), contrast-to-noise ratio (CNR), and contrast recovery coefficient (CRC). These parameters are widely accepted as fundamental evaluation criteria in performance assessment protocols, such as those recommended by the National Electrical Manufacturers Association (NEMA) [6].

In PET systems, contrast reflects how distinctly radiotracer uptake in the target area is visualized relative to its surroundings. Higher contrast increases lesion visibility. However, contrast alone is not sufficient; image noise also must be considered. The CNR allows for a combined assessment of contrast and image noise, and provides a more realistic measure of the target's detectability against the background.

In 2025, Bharathi et al. [7] reported that AI-based PET image reconstruction techniques contribute to noise reduction and overall image quality improvement, supporting their potential role in future dose-reduction and activity-optimization strategies [7, 8].

The higher the CNR, the easier it is to distinguish lesions within the image. This metric becomes particularly important in low-dose imaging protocols or when detecting small lesions [9].

As the technology for long-axial field-of-view PET becomes more accessible, the total-body concept gains relevance for both clinical and research applications. These systems demonstrate remarkable potential for low-dose imaging, faster acquisitions, and whole-body dynamic scanning over extended timeframes, thereby expanding kinetic modeling capabilities. In addition, studies published in 2021 in *Phys. Med. Biol.* highlight the benefit of reconstruction optimization strategies for improving quantitative accuracy in dynamic and low-count imaging conditions [10, 11].

Historically, CNR thresholds in the range of 3–5 have been proposed as a measure of detectability. More recent studies commonly employ the Rose criterion, which defines the detectability threshold as CNR ≥ 5 [12–15].

The CRC expresses the system's ability to accurately quantify the true concentration of activity within a lesion, expressed as a percentage. This metric is particularly relevant for evaluating partial volume effects (PVE), especially in small-volume lesions. PVE is a complex phenomenon influenced by tumor size and shape, background activity, scanner spatial resolution, voxel size, and reconstruction technique. It refers to the tendency of imaging systems to underestimate the activity of small lesions due to limited spatial resolution, visualizing them as larger and with diminished activity. In clinical oncologic studies using ^{18}F-FDG, PVE correction typically accounts for 'spill-out' from the lesion to the background, but not the 'spill-in' from the background to the lesion. Therefore, realistic models where the lesion is surrounded by relatively lower activity have been developed. PET NEMA IQ phantoms were specifically designed to simulate such conditions, incorporating both 'spill-out' and 'spill-in' effects into evaluation [16]. A CRC [%] value closer to 100% indicates better activity recovery performance. In small lesions, lower CRC values are expected, reflecting the limitations of spatial resolution and dependence on reconstruction algorithms.

The aim of this study was to evaluate image quality in a PET NEMA IQ phantom using ^{18}F-FDG at different signal-to-background (S/Bg) ratios and varying activity concentrations, and to determine the minimum detectable lesion size.

2. Materials and methods

2.1. NEMA image quality testing and imaging system

The NEMA image quality tests in this study were conducted using a GE Discovery 690 model PET/CT system (GE — General Electric).

2.2. Phantom preparation and imaging

The PET NEMA 2012/IEC 2008 image quality phantom is made of Plexiglas with a water equivalent density coefficient (1.18 g/cm^3) and contains spheres of various inner diameters (10, 13, 17, 22, 28, and 37 mm). A low-density central insert (0.3 g/cm^3), filled with styrofoam, simulates lung tissue. The total phantom volume is 9.7 l and was filled with water mixed with a homogeneous concentration of ^{18}F-FDG at 5.18 kBq/ml. The hot spheres in the phantom served as the signal, and the remaining volume was defined as the background (Bg). The phantom was filled with three different signal-to-background (S/Bg) ratios: 4:1, 6:1, and 8:1. Two larger spheres (28 and 37 mm in diameter), referred to as 'cold lesions,' were filled only with water.

The activity concentrations of the lesions at the start of imaging were 9.90, 9.85, and 9.82 MBq/kg for S/Bg ratios of 4:1, 6:1, and 8:1, respectively, while keeping the contrast ratios constant. The time intervals between consecutive acquisitions ranged from a minimum of 44 min to a maximum of 52 min, with a mean of 48 min, and were kept as consistent as possible. The activity concentrations of ^{18}F-FDG

injected into the phantom were measured using a Biodex Atomlab 500 dose calibrator. The linearity deviation of the dose calibrator was ±1.89%.

Following preparation at each S/Bg ratio (i.e., 4:1, 6:1, and 8:1), the phantom was placed on the patient table and scanned for 2 min in a single bed position. To allow for radioactive decay, a waiting period of ≈ 48 min was applied between successive acquisitions. After this interval, imaging was repeated using the same acquisition parameters. Images were acquired using a 256 × 256 matrix and a display field of view (DFOV) of 40 cm. Reconstruction was performed using the VPHD (VUE Point HD) reconstruction type with a 2 mm post-filter cutoff, 8 iterations, and 12 subsets of the ordered subset expectation maximization (OSEM) algorithm. CT acquisition parameters were as follows: helical scan type, full rotation, tube voltage of 120 kV, rotation time of 0.2 s, slice thickness of 3.75 mm, and DFOV of 70 cm.

2.3. Image acquisition parameters and quantification

For quantitative analysis, regions of interest (ROI) matching the internal volume of each hot sphere were drawn directly on the spheres. Additionally, twelve spherical background ROIs were placed in the same transaxial plane as the hot spheres.

For hot spheres in the PET NEMA phantom, contrast (C) and contrast-to-noise ratio (CNR) were calculated using, respectively,

$$\text{contrast (C)} = \frac{N_{\mathrm{L}} - N_{\mathrm{B}}}{N_{\mathrm{B}}}, \tag{1}$$

and

$$\text{CNR} = \frac{N_{\mathrm{L}} - N_{\mathrm{B}}}{\sigma_{\mathrm{B}}}, \tag{2}$$

where N_{B} is the mean pixel value of the background ROIs, σ_{B} is the standard deviation of the background ROIs, and N_{L} is the mean pixel value within the lesion ROI [17]. Both (1) and (2) were described earlier in [18].

The detectability of lesions is not limited solely by lesion size and signal-to-background (S/Bg) ratio, but is also directly related to the spatial resolution of the PET system. Spatial resolution is defined by the point spread function (PSF); the narrower the PSF, the higher the contrast of small lesions, and thus, the greater the detectability. Particularly, lesions with diameters of 10–13 mm are directly affected by PSF and partial volume effects (PVE) [19, 20].

Therefore, the lesion detection thresholds determined in the present study may have been constrained by the PSF, and enhancing contrast through the use of PSF-based reconstruction algorithms could improve the detectability of small lesions. In this study, PET IQ images were processed using ordered subsets expectation maximization (OSEM) algorithms. The standard OSEM algorithm reconstructs PET images iteratively but does not directly account for the PSF. However, to reduce the effects of PSF and improve image quality, PSF modeling can be integrated into the OSEM algorithm. Such integration is particularly beneficial for detecting small lesions and increasing image contrast. The standard OSEM algorithm was used in this study. Nevertheless, previous studies have demonstrated that incorporating PSF modeling into the OSEM algorithm enhances image resolution and improves the detectability of small lesions [21–23]. Hence, in future studies, integrating PSF modeling into the OSEM algorithm may further improve image quality.

The contrast recovery coefficient (CRC) indicates how accurately the activity concentration within a specific volume is measured in PET images and can therefore be used to assess image quality. Theoretically, the CRC value should be equal to 1. However, a CRC values greater than 1 indicates higher image quality. For spherical volumes, CRC can be defined as follows

$$\text{CRC } [\%] = \frac{(C_{\mathrm{H}}/C_{\mathrm{B}}) - 1}{(a_{\mathrm{H}}/a_{\mathrm{B}}) - 1} \times 100, \tag{3}$$

where C_{H} is the mean count within the ROI drawn on the hot sphere, C_{B} is the mean count in the background ROI, a_{H} is the activity concentration in the hot sphere, and a_{B} is the activity concentration in the background. CRC values were calculated in accordance with the research direction presented by X. Su et al. [24] and with the NEMA NU-2018 criteria (see (3)) [24, 25].

3. Results and discussion

In this study, a PET/CT system was used to perform sequential imaging of a PET NEMA phantom filled with ^{18}F-FDG radiopharmaceutical at lesion-to-background (L/Bg) ratios of 4:1, 6:1, and 8:1, with activity concentrations decreasing over time. Contrast, CNR, and CRC [%] values were calculated. To provide a reference for clinical PET applications, the effect of varying patient doses in MBq/kg on image quality at these different L/Bg ratios was also investigated. Thus, the combined impact of changes in lesion-to-background ratio and patient dose [MBq/kg] on image quality was assessed.

In the experiments conducted in this study, the PET NEMA 2012/IEC 2008 phantom was used. PET images acquired at different S/Bg ratios filled into the phantom are shown in Fig. 1. The six corresponding activity concentration values for L/Bg ratios of 4:1, 6:1, and 8:1 are presented in Table I. The activity concentrations were at their highest levels

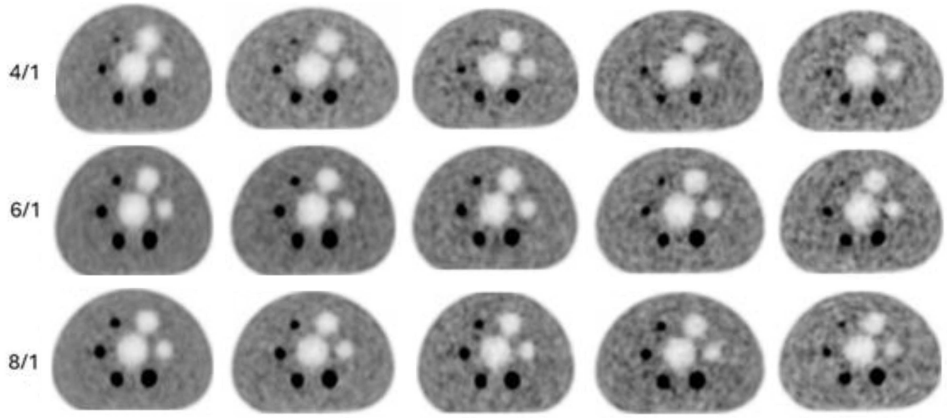

Fig. 1. PET phantom images at different S/Bg ratios and varying activity concentrations.

TABLE I

Administered ^{18}F-FDG activity concentrations in the phantom.

L/Bg	Activity concentration [MBq/kg]					
4:1	9.96	7.34	5.51	3.90	2.89	2.02
6:1	9.98	7.14	5.29	3.82	2.76	1.93
8:1	9.92	7.37	5.48	3.73	2.79	1.96

at the beginning of the acquisition, and the average interval between consecutive scans was 48 min. During this period, the activity of ^{18}F decreased, and in the later acquisitions, the 10 mm diameter hot lesion was no longer visible at concentrations below 5.51 MBq/kg for the 4:1 ratio and at 1.93 MBq/kg for the 6:1 ratio. For the 8:1 ratio, the lesion was partially visible at an activity concentration of 1.96 MBq/kg.

Detection limits of tumors in clinical conditions vary depending on multiple parameters. Clinical studies in nuclear medicine indicate that the minimum detectable lesion — assuming a spherical shape — is approximately 1.5 cm in diameter, corresponding to a lesion volume of 1.77 ml [26]. Hashimoto et al. [27] demonstrated that time of flight (TOF)-based reconstruction and the use of small voxel sizes significantly improve the detectability of sub-centimeter hot spheres ($\leq$ 10 mm) in PET/CT systems at an 8:1 lesion-to-background ratio. Erdi et al. [28] reported that PET imaging improved tumor detectability by almost an order of magnitude due to a sharp decrease in full width at half maximum (FWHM). They also noted that when the imaged object is at least twice the width of the system's FWHM, the object contrast is accurately reproduced by the system. Fukukita et al. [29] reported that detecting a 10-mm hot sphere in PET/CT is challenging due to limited spatial resolution and count statistics, and emphasized that acquisition protocols must be optimized according

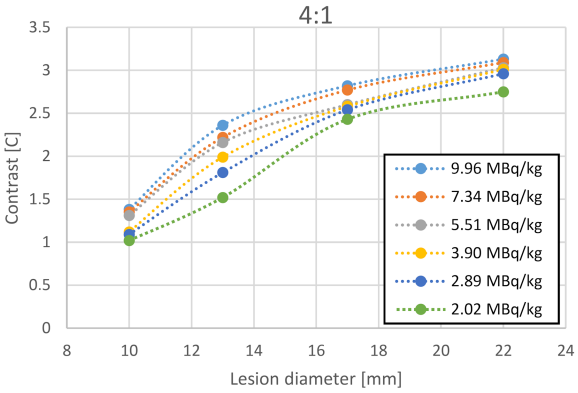

Fig. 2. Variation of contrast values for an L/Bg ratio of 4:1 depending on lesion diameter and activity concentration.

to clinical requirements and operational constraints. They also cautioned that results from hot-sphere phantom experiments cannot be directly extrapolated to patients with varying body thicknesses.

With increasing ^{18}F activity concentration and lesion diameter, a corresponding increase in lesion contrast was observed. For an L/Bg ratio of 4:1, the highest contrast was obtained in a lesion with a diameter of 22 mm, while, as expected, the lowest contrast was observed in a lesion with a diameter of 10 mm (Fig. 2).

The contrast values for a 6:1 ratio are shown in Fig. 3. It can be observed that contrast tends to increase more noticeably as the lesion diameter increases.

The contrast variation with respect to lesion diameter for an 8:1 ratio is shown in Fig. 4. As expected, this figure also demonstrates that the contrast increases as the lesion diameter increases.

At an L/Bg 4:1 ratio, CNR values fall below 5 at activity concentrations of 3.73 MBq/kg and lower, indicating that the lesions are below the detection threshold (Fig. 5).

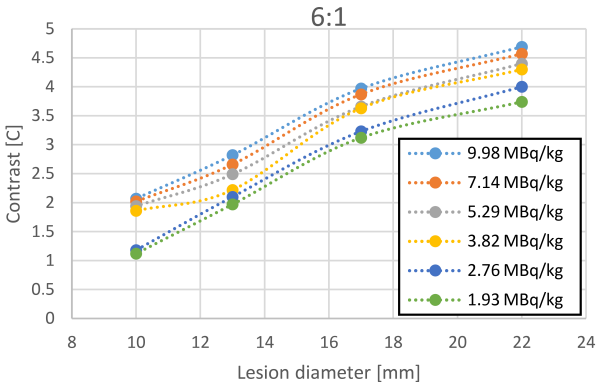

Fig. 3. Variation of contrast values for a 6:1 ratio depending on lesion diameter and activity concentration.

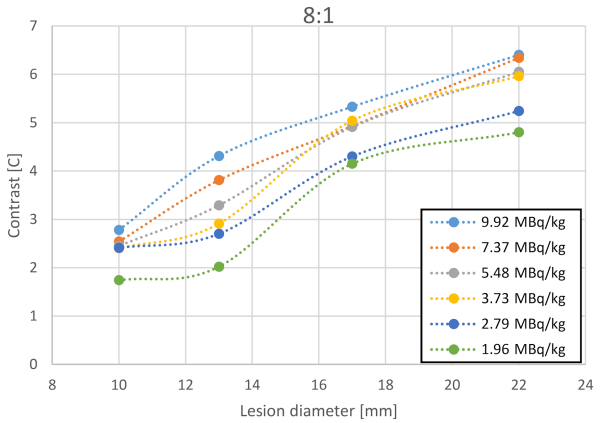

Fig. 4. Variation of contrast values for an 8:1 ratio depending on lesion diameter and activity concentration.

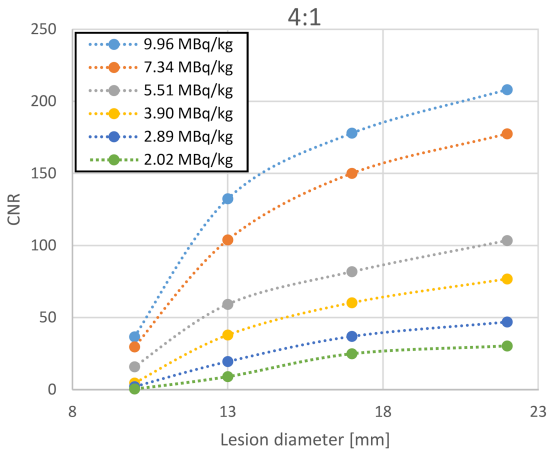

Fig. 5. Variation of CNR values depending on lesion diameter for a 4:1 ratio.

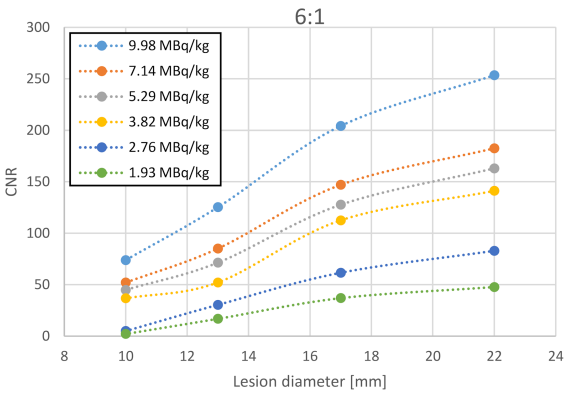

Fig. 6. Variation of CNR values depending on lesion diameter for a 6:1 ratio.

At an L/Bg 6:1 ratio, CNR values fall below 5 for the 10 mm diameter lesion at activity concentrations of 2.76 MBq/kg and lower, indicating that the lesion is below the detection threshold (Fig. 6).

At an L/Bg 8:1 ratio, the CNR values of all lesions were found to be greater than 5.

Our findings demonstrated that for all ratios, contrast values increased with increasing activity concentration and lesion diameter. For example, at a 4:1 ratio for a 10 mm lesion, the lowest activity concentration with CNR < 5 was 3.3 MBq/kg, where the contrast was 1.12; at 4.81 MBq/kg, the contrast increased to 1.31. This corresponds to a 32% increase in activity concentration, yielding a 15% improvement in contrast.

Despite the many factors influencing lesion detectability, CNR was chosen as a practical and well-established metric. An early study by Rose [13] recommended an CNR threshold of around 5 for object detectability. Since then, various alternative detection indices and observer models have been proposed, many of which correlate well with human observer results [15, 30, 31].

In addition to the NEMA standard of using a 10 mm sphere as the smallest lesion for PET image quality evaluation, upgrades to current PET imaging guidelines and standardized image quality phantoms are needed to meet the requirements of modern PET systems. In our study, the highest CNR values, as expected, were observed at an activity concentration of 9.99 MBq/kg with an 8:1 ratio, reaching 104.42. For 6:1 and 4:1 ratios, the CNR values were 73.88 and 36.7, respectively. When designing PET for clinical applications, the European Association of Nuclear Medicine (EANM) guidelines recommend adult patient ^{18}F-FDG doses of 14 MBq/kg for PET bed overlap $\leq 30\%$ and of 7 MBq/kg for PET bed overlap $> 30\%$ [32].

Consistent with our phantom observations at lower activity levels, Bharathi et al. [7] reported that AI-assisted (deep learning) PET reconstruction can suppress image noise and enhance overall image quality while preserving spatial detail, thereby supporting more reliable contrast and CNR under low-count conditions. Silosky et al. [15] conducted a ^{68}Ga PET phantom study, reporting that

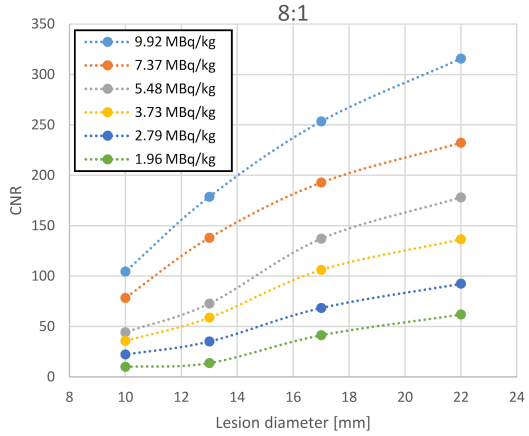

Fig. 7. Variation of CNR values depending on lesion diameter for an 8:1 ratio.

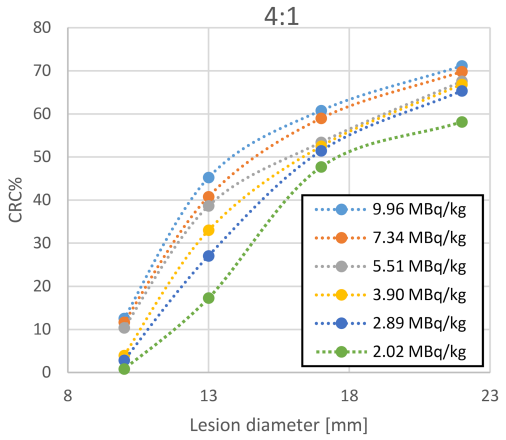

Fig. 8. Variation of CRC [%] values depending on lesion diameter for a 4:1 ratio.

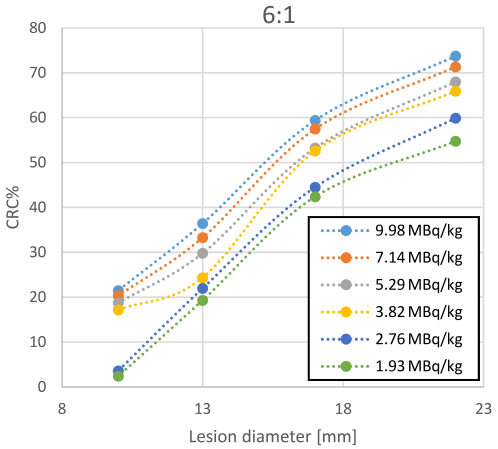

Fig. 9. Variation of CRC [%] values depending on lesion diameter for a 6:1 ratio.

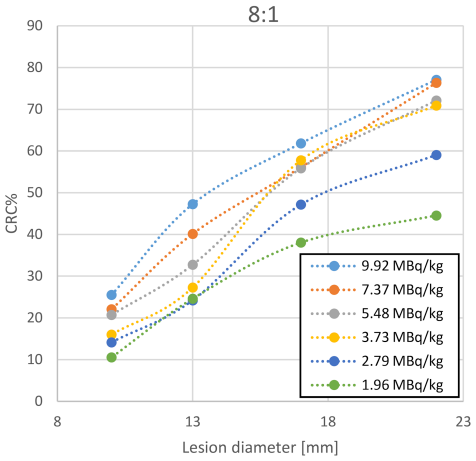

Fig. 10. Variation of CRC [%] values depending on lesion diameter for an 8:1 ratio.

increasing imaging time to improve counts for small (8 mm) targets with low uptake (standardized uptake value SUV = 2.4) did not significantly enhance CNR. Increasing imaging time by 300% (from 5 to 15 min) raised CNR only from less than 1 to 1.6. However, increasing the lesion-to-background ratio substantially improved CNR [15]. In our study, CNR values were found to be below 5 at activity concentrations less than 3.3 MBq/kg for a 4:1 ratio and less than 2.96 MBq/kg for a 6:1 ratio.

According to the manufacturer's specifications, the CRC [%] values for lesions with diameters of 22, 17, 13, and 10 mm are reported as 50%, 40%, 30%, and 20%, respectively. Accordingly, for a 4:1 ratio, the 13 mm diameter lesion remains below the limits after an activity concentration of < 2.89 MBq/kg. The 10 mm diameter lesion remains below the limits at all examined activity concentrations (< 9.96 MBq/kg) (Fig. 8).

At a 6:1 ratio, the CRC [%] values for the 10 mm diameter lesion remain outside the limits at activity concentrations below 5.29 MBq/kg. Similarly, for the 13 mm diameter lesion, the CRC [%] values remain outside the limits at activity concentrations below 3.82 MBq/kg (Fig. 9).

At an 8:1 ratio, the CRC [%] values for all lesions were found to be above the limits. For the 13 mm diameter lesion, the CRC [%] values remain outside the limits at activity concentrations below 3.82 MBq/kg (Fig. 10).

Regression analysis was performed between the S/Bg ratios of 4:1 and 6:1, 4:1 and 8:1, and 6:1 and 8:1, and the coefficient of determination (R^2) was found to be $R^2 = 0.8359$, $R^2 = 0.8476$, and $R^2 = 0.9448$, respectively. Among these results, the correlation between 6:1 and 8:1 is stronger than the others.

Partial volume effect (PVE) occurs due to the finite spatial resolution of PET imaging systems, causing spill-over of radioactivity from adjacent regions and reducing the visibility of small lesions [33]. Blur caused by spatial resolution decreases image contrast, limiting the detectability of small

lesion [34]. Among PVE correction methods, contrast recovery coefficients (CRCs) — multiplicative numerical factors — are the simplest and most practical for clinical use. They are defined as the ratio of measured PET radioactivity to true radioactivity within spheres [35]. CRCs are obtained experimentally using phantoms and radionuclides mimicking small anatomical structures, typically spherical objects of known size and activity placed in a background medium [36]. Fukukita et al. [29] reported CRC [%] values at a 4:1 ratio and 2.65 MBq/kg activity concentration for lesions of 10, 13, 17, and 22 mm diameters as 38, 52, 72, and 88, respectively [29]. In our study, CRC [%] values fell below reference limits after 7.7 MBq/kg at 4:1, after 2.96 MBq/kg at 6:1, and after 1.48 MBq/kg at 8:1. Krempser et al. [36], evaluating image quality with a PET NEMA phantom, reported CRC [%] values at 5.3 MBq/kg and 4:1 ratio for 22, 17, 13, and 10 mm spheres as 91, 79, 65, and 27, respectively [36]. Compared with our findings at 4:1 and 4.81 MBq/kg, CRC [%] values were 68, 53, 39, and 10. Bettinardi et al. [18] noted that PVE affects small and hot lesions and that PVE correction using recovery coefficients is possible, but the impact on detectability in small lesions is minimal [16].

In phantom studies focusing on NEMA IQ protocols, it has been shown that increasing the β parameter in the Q.Clear reconstruction algorithm enhances image uniformity, but at the cost of reduced SUV as well as CRC values — particularly under conditions of lower activity and small lesion size. This indicates that reconstruction parameter tuning plays a decisive role when activity is reduced, as contrast recovery performance becomes increasingly sensitive to noise regularization [37]. In our study, CRC [%] values exceeded manufacturer limits across all lesion-to-background ratios.

4. Conclusions

Ensuring consistent phantom preparation is vital to determine the minimum lesion detectability of a PET system. Therefore, at the start of each scan at different lesion-to-background ratios, the same signal-to-background concentration ratio and absolute activity in the field of view were maintained. The major strength of this study is that multiple scans were performed at S/Bg ratios of 4:1, 6:1, and 8:1. This allowed for the determination of the minimum detectable activity concentration for each ratio by varying the activity concentration without changing the ratio.

In this study:

- An activity concentration threshold was proposed for lesion detectability in 90Y microsphere PET imaging, particularly for liver lesions with low tumor-to-background ratios.
- The limits of CRC [%] values in partial volume effect (PVE) correction were evaluated.

Regarding the limitations of this study, it should be noted that image quality evaluations at decreasing activity concentrations were conducted on only one PET model. It is recommended to perform similar studies using different PET devices from various manufacturers and models.

References

[1] S. Yu, *Biomed. Imaging Interv. J.* **2**, e57 (2006).

[2] J.M. Chang, H.J. Lee, J.M. Goo, H.-Y. Lee, J.J. Lee, J.-K. Chung, J.-G. Im, *Korean J. Radiol.* **7**, 57 (2006).

[3] S. Vandenberghe, P. Moskal, J.S. Karp, *EJNMMI Phys.* **7**, 35 (2020).

[4] A. Braune, L. Oehme, R. Freudenberg, F. Hofheinz, J. van den Hoff, J. Kotzerke, S. Hoberück, *EJNMMI Phys.* **9**, 58 (2022).

[5] P. Kopka, K. Klimaszewski, *Acta Phys. Pol. B* **51**, 357 (2020).

[6] G. Yılmaz, A.B Tuğrul, M. Demir, D. Yaşar, B. Demir, *Acta Phys. Pol. A* **130**, 90 (2016).

[7] P.G. Bharathi, S. Abbaszadeh, A. Alavi, P. Moskal, *Bio-Algorithms Med-Syst.* **21**, 40 (2025).

[8] A. Alavi, T.J. Werner, E.Ł. Stępień, P. Moskal, *Bio-Algorithms Med-Syst.* **17**, 203 (2022).

[9] R. Boellaard, *J. Nucl. Med.* **50**, 11S (2009).

[10] S. Vandenberghe, P. Moskal, J.S. Karp, *EJNMMI Phys.* **7**, 35 (2020).

[11] P. Moskal, P. Kowalski, R.Y. Shopa et al., *Phys. Med. Biol.* **66**, 175015 (2021).

[12] M. Nachiappan, A. Cai, M. Silosky, B. Chin, *J. Nucl. Med.* **65**, 242071 (2024).

[13] A. Rose, in: *Vision — Human and Electronic*, Springer, Boston (MA) 1973, p. 1.

[14] S. Adler, J. Seidel, P. Choyke, M.V. Knopp, K. Binzel, J. Zhang, C. Barker, S. Conant, R. Maass-Moreno, *EJNMMI Phys.* **4**, 13 (2017).

[15] M. S.Silosky, R. Karki, R. Morgan, J. Anderson, B.B. Chin, *Am. J. Nucl. Med. Mol. Imaging* **11**, 27 (2021).

[16] K.A. Wangerin, S. Ahn, S. Wollenweber, S.G. Ross, P.E. Kinahan, R.M. Manjeshwar, *J. Med. Imaging* **4**, 011002 (2017).

[17] Z. Gong, K. Klanian, T. Patel, O. Sullivan, M.B. Williams, *Med. Phys.* **39**, 7580 (2012).

[18] V. Bettinardi, I. Castiglioni, E. De Bernardi, M.C. Gilardi, *Clin. Transl. Imaging* **2**, 199 (2014).

[19] M.L. Giger, H.-P. Chan, J. Boone, *Med. Phys.* **35**, 5799 (2008).

[20] M. Soret, P.M. Koulibaly, J. Darcourt, S. Hapdey, I. Buvat, *J. Nucl. Med.* **44**, 1184 (2003).

[21] J. Zhao, Y. Song, Q. Liu, S. Chen, J.-C. Chen, *Electronics* **12**, 1309 (2023).

[22] E. Rapisarda, V. Bettinardi, K. Thielemans, M.C. Gilardi, *Phys. Med. Biol.* **55**, 4131 (2010).

[23] T. Murata, K. Miwa, N. Miyaji et al., *EJNMMI Phys.* **3**, 26 (2016).

[24] X. Su, J. Geng, J. Liu, F. Liu, Y. Wu, R. Zheng, X. Wang, *Radiat. Detect. Technol. Methods* **8**, 1171–1186 (2024).

[25] National Electrical Manufacturers Association, "Performance Measurements of Positron Emission Tomographs (PETS)", NU 2-2018, NEMA, Rosslyn (VA) 2018.

[26] A.K. Erdi, Y.E. Erdi, E.D. Yorke, B.W. Wessels, *Phys. Med. Biol.* **41**, 2009 (1996).

[27] N. Hashimoto, K. Morita, Y. Tsutsui, K. Himuro, S. Baba, M. Sasaki, *J. Nucl. Med. Technol.* **46**, 268 (2018).

[28] Y.E. Erdi, Mol. Imaging, *Radionucl. Ther.* **21**, 23 (2012).

[29] H. Fukukita, K. Suzuki, K. Matsumoto, T. Terauchi, H. Daisaki, Y. Ikari, N. Shimada, M. Senda, *Ann. Nucl. Med.* **28**, 693 (2014).

[30] H.H. Barrett, J. Yao, J.P. Rolland, K.J.Myers, *Proc. Natl. Acad. Sci. U.S.A.* **90**, 9758 (1993).

[31] J.D. Schaefferkoetter, J. Yan, T. Sjöholm, D.W. Townsend, M. Conti, J.K.C. Tam, R.A. Soo, I. Tham, *J. Nucl. Med.* **58**, 399 (2017).

[32] R. Boellaard, R. Delgado-Bolton, W.J.G. Oyen et al., *Eur. J. Nucl. Med. Mol. Imaging* **42**, 328 (2015).

[33] O.G. Rousset, H. Zaidi, in: *Quantitative Analysis in Nuclear Medicine Imaging*, Ed. H. Zaidi, Springer, New York (NY) 2006, p. 236.

[34] O. Rousset, A. Rahmim, A. Alavi, H. Zaidi, *PET Clinics* **2**, 235 (2007).

[35] N.J. Hoetjes, F.H. van Velden, O.S. Hoekstra, C.J. Hoekstra, N.C. Krak, A.A. Lammertsma, R. Boellaard, *Eur. J. Nucl. Med. Mol. Imaging* **37**, 1679 (2010).

[36] A.R. Krempser, R.M. Ichinose, A.M. Miranda de Sá, S.M. Velasques de Oliveira, M.P. Carneiro, *Ann. Nucl. Med.* **27**, 924 (2013).

[37] K. Skórkiewicz, K. Łątka, K. Sowa-Staszczak, A. Hubalewska-Dydejczyk, *Bio-Algorithms Med-Syst.* **19**, 17 (2023).